Version of Record: https://www.sciencedirect.com/science/article/pii/S0038092X18309733
Manuscript_1a16eaf557d02fc6c8e82590f53bb0b5

Thermal Impact of Adhesive-Mounted Rooftop PV on Underlying Roof Shingles

Nitin Shukla*, Alliston Watts, Christian Honeker, Mark Hill, Jan Kośny

Fraunhofer Center for Sustainable Energy Systems CSE, Boston, MA, USA

* Corresponding Author; e-mail address: nshukla@cse.fraunhofer.org (N. Shukla)

1 Abstract

Adhesive mounting of residential rooftop photovoltaics (PV) is an alternative to traditional rack mounting that reduces installation costs. Adhesive mounting is fast, simple and reduces the need for skilled labor. In our novel design that further reduces the installation costs, a lightweight (glassless and frameless) PV module is directly adhered to a shingled roof using an adhesive tape, creating a <5 mm air gap between the PV back-panel and the roof shingle surface. Although the gap is sufficient for moisture and rainwater transport under the PV panel, potential heat buildup under the module may adversely impact the long-term durability of the shingles. Heat buildup may also increase the heat flux through the roof, resulting in an overall increase in building cooling loads. This study investigates the thermal behavior of the roof under an adhered PV system. Two identical test huts with dark shingle-covered roofs were located in the hot, desert climate of Albuquerque, NM. Adhesively-mounted lightweight PV modules were installed on the south-facing roof of one of the test huts (PV hut), with the other one serving as a reference hut. During the summer season, the asphalt roof shingles under the PV modules experienced a 13°C reduction in daytime peak temperature compared with the exposed shingles. No evidence of heat buildup under the PV module was observed. It was also found that the temperature of shingles underneath the adhesive was up to 6°C higher than for shingles underneath the gap space at the daily peak time. Thin but ventilated air gap between the PV back-panel and the roof shingles helped remove the heat, while the adhesive pads (patches) served as thermal bridges between the PV module and the roof. Daily peak heat flow through the attic ceiling was almost 49% lower in the PV hut compared to the reference hut. These results show no evidence of an adverse thermal impact of the adhesive-mounted PV system on the roofing materials, while demonstrating a potential for a notable reduction in space conditioning energy requirements.

2 Introduction

Substantial reductions in the PV module cost in recent years has fueled a rapid rise in US residential rooftop PV installations. In 2015, the residential PV installations exceeded 2 GW (Kann *et al*., 2015). By comparison, the National Removable Energy Laboratory (NREL) estimates that the technical potential for residential PV in the US is approximately 731 GW (Gagnon *et al*., 2016). To realize this huge market potential, however, the non-hardware (soft) material and installation costs must be reduced (Ardani *et al*., 2013; Barbose *et al*., 2013; Morris *et al*., 2013; Morris *et al*., 2014). These soft costs remain higher in the US than in most other countries, due in part to a higher cost of installation and complicated code approvals (Barbose & Darghouth, 2015). Traditional rack-mounting of PV modules on the residential roofs is both time and skill intensive and involves: drilling mounting holes into the roof, attaching and flashing the mounts, attaching rails to the mounts, and securing PV modules to the rails. The complexity

and cost of rail-based mounting has led to an increase in popularity of rail-less mounting methods (Harris, 2016). However, both mounting approaches require roof penetration, which increases the risk of moisture damage to the building.

In a United States Department of Energy (US DOE) funded Plug and Play project, we investigated the adhesive mounting of lightweight (glass-less, frame-less) PV modules as a mean to reduce the soft costs (Fraunhofer CSE, 2016; Honeker *et al*., 2016). The use of adhesives to attach lightweight PV modules directly to a residential roof has the advantages of speed, simplicity and reduction of skilled labor. By removing the frame and the glass frontsheet, the resulting lightweight module is well suited for adhesive mounting and may not require structural permitting which is both time consuming and adds to the installation cost. The design of this frame- and rack-less PV system does not include any metal component, which avoids the need for electrical grounding, saving on the associated materials and electrician labor cost.

To ensure the sufficient structural integrity, we studied the wind uplift, creep performance and durability of the adhesives (Honeker *et al*., 2016). Wind uplift tests performed in the wind-tunnel suggest that, properly installed, the adhered modules can withstand wind gusts up to 150 mph. During field exposure tests performed in Albuquerque, NM, it was found that, a slow displacement of the module over time (creep), may occur under extreme conditions of high angle, high temperature and high loads. Finally, a series of adhesive durability tests performed in climatic chambers, demonstrate that the thermoplastic adhesive bond gains strength on exposure to high temperatures as temperature facilitates the adhesive's ability to wet into the granulated shingle surface.

To examine the impact of adhesively-mounted rooftop lightweight PV on the moisture transport of the underlying roof elements, we conducted an outdoor test hut study in cold, humid climate of Boston, MA (Shukla *et al*., in publication). Lightweight PV modules were attached using 0.15 cm (0.6 in.) thick adhesives and covered approximately half of North and South roofs of the test hut. Moisture content data collected over two winter periods showed no adverse effect of the adhesively-mounted PV on the hygrothermal behavior of the underlying roof deck element.

A series of field experiments focused on the thermal effects of adhesive mounting on the PV module electric performance were performed in Albuquerque, NM (Beutner *et al*., unpublished). The study compared the temperature and power output of glass/glass modules mounted at gaps of 17.78 cm (7 in.), 10.16 cm (4 in.) and 0.32 cm (0.125 in.) (adhesive) on the test huts. The recorded average annual temperature of adhesively mounted glass/glass module was found to be 3.4°C and 4.3°C higher than the 10.16 cm (4 in.) gap and 17.78 cm (7 in.) gap mounted modules, respectively. This temperature increase resulted in an average annual yield loss of 4% and 6.5%, respectively. To complement the above study, this study focuses on the effects of adhesive mounting on the roof temperature and building cooling loads.

In a conventional rail-based rack-mounted PV system, a >10 cm gap between the roof surface and the module back surface enables significant air convection under the panel, minimizing heat build-up (Brinkworth & Sandberg, 2006; Gan, 2009a; Gan, 2009b; Hirunlabh *et al*., 2001). In addition, conventional rack-mounted PV modules act as roof sunshades by blocking the incident sunlight. In contrast, adhesive-mounting leaves a < 0.5 cm gap between module back-surface and roof shingles. From building physics viewpoint, there is a concern that this small gap limits the air-flow below the PV module, which will result in heating of the roof surface i.e. roof shingles. Increased temperatures are known to accelerate the degradation and reduce service life of common types of shingle materials used

today such as asphalt shingles. Although adhesive-mounting of PV systems on flat commercial membrane roofs and sloped metal roofs is well-known (Uni-Solar, 2015), few data exists on the thermal effects of the adhesively-mounted PVs on residential roofs.

3 Technology Background

Compared with conventionally rack-mounted framed PV modules, the adhesively-mounted lightweight (frameless, glassless) PV modules are expected to alter the heat transport through the roof because of the following reasons:

(a) reduced air gap thickness between the PV and shingles in the adhesive-mounted modules compared to the rack-mounted approach may reduce the convective heat transfer underneath the PV module
(b) different surface radiative characteristics (emissivity and reflectivity) of the polymeric frontsheet of the lightweight PV module, compared with the glass frontsheet of the conventional framed module
(c) local thermal bridging caused by the adhesive pads

These heat transfer mechanisms may increase the temperature of the roof under the adhered PV module. Please note that the excessive shingle temperatures may accelerate their degradation by increasing oil migration and asphalt oxidation (ARMA, 1996; Berdahl, *et al*., 2008; Cash, 2000; Terrenzio *et al*., 1998). In addition, since a typical roof accounts for about 14% of the total cooling loads in a residential building (Buildings Energy Databook, 2010), the potential for heat build-up caused by adhesive-mounted rooftop PV may increase the cooling demand of the building. A further PV performance-affecting factor is the conversion of a portion of the solar radiation to electricity (PV effect). Since an increase in temperature reduces PV cell efficiency (Dubey *et al*., 2013), many studies have investigated the thermal effects of PV system design parameters (including gap spacing, aspect ratio, radiation properties etc.) on the rooftop PV module performance (Beutner *et al*., unpublished; Hirunlabh *et al*., 2001; Singh *et al*., Gran, 2009a; Moshfegh & Sandberg, 1998; Sandberg & Moshfegh, 1998; Wilson *et al*., 2011). In contrast, fewer studies are available on the thermal impacts of rooftop PV systems on underlying roof elements. Generally, the literature shows that rack-mounted PV systems shade the building envelope, resulting in reduced building cooling loads.

Yang *et al.* (2001) have simulated the effect of gap spacing on the temperature and performance of rooftop PV systems. Natural ventilation was found to remove a large amount of heat, reducing the building cooling demand. The roof thermal load decreased by almost 35% with the application of rooftop PV. Tian *et al.* (2007) modeled the effect of PV systems on the microclimate of the urban canopy layer. Simulations for Tianjin, China showed that PV systems with ventilating gaps significantly reduce roof surface temperature and heat flux density through the roof envelope compared to roofs without PV during the daytime; night differences were found to be small.

Kośny *et al.* (2012) performed a field study to investigate the thermal performance of a novel roofing technology utilizing amorphous silicon PV laminates integrated with the metal roof panels. The system featured phase change material (PCM), a ventilated channel over the roof deck and thermal insulation with an integrated reflective layer to suppress thermal bridging and reduce thermal loads through the roof. The test results showed an approximately 90% reduction in peak daytime roof heat flux and a 55%

reduction in roof-generated cooling loads compared to a shingle roof control. However, no attempts were made to isolate the impact of PV laminates on the thermal performance.

Trinuruk *et al.* (2007) investigated the effect of a completely enclosed gap below a PV panel, which represents a worst-case condition from the standpoint of PV performance, on the heat flux through the underlying building envelope component. At 15° tilt (latitude in Thailand) and low wind speed, results indicated that air gaps larger than 4 cm were needed to reduce the heat transfer from the back of the PV modules to the envelope component. It was concluded that an appropriate air gap could reduce the heat load of the building by at least 1.85 kWh/m^2 per year. Bigot *et al.* (2009) investigated the effect of PV rooftop panels on the roof-generated heat loads of a building in tropical and humid climate of La Reunion Island. Ceiling temperature was reduced by up to 6°C and roof thermal loads were decreased by ~51% under a PV-covered roof compared with a non-covered roof.

Samady (2011) used small-scale building models to compare the thermal behavior of roofs with different PV designs. Two designs are of particular interest: 1) a flush-mounted system with no air gap and 2) a rail-mounted system with a 7.6 cm gap. The roof temperature of the flush-mounted system was significantly higher than the system with the gap. In fact, the roof temperature of flush-mounted system was found to be even higher than the exposed (uncovered) roof temperature. The temperature differences between the roof surface and the ceiling were higher for the flush roof compared to the roof with gap, indicating higher thermal loads in the flush roof case. Further analysis showed that the flush mounting yielded about 60% higher cooling load than the design with the 7.6 cm gap.

Dominguez *et al.* (2011) demonstrated the behavior of rooftop PV systems as thermal insulation on a commercial building in San Diego, California. Two PV designs were studied: a flush-mounted system and a south-facing tilted system with a 4° tilt and a 10 cm gap. Thermal (infrared) imaging showed that the ceiling under both designs was cooler than the ceiling under the exposed (uncovered) roof surface, with the tilted design showing a higher maximum daytime cooling of about 2.5°C. Numerical simulations showed an approximately 38% reduction in annual cooling load due to the PV systems as compared to the exposed roof. No benefits in annual heating load were noted.

Mei *et al.* (2009) performed laboratory tests to assess the risk of overheating of PV tiled roofs. An excessive rise in PV tile temperature was reported under the indoor test conditions, which was attributed to inability of the applied test arrangement to simulate a realistic level of radiative cooling to the sky. Locations within Southern Europe that have the potential for overheating of PV roof tile designs with no back ventilation were identified. Numerical analysis showed that using counter batten helps in reducing the PV roof tile temperature by 3°C by providing air-flow convection.

In summary, the literature on the thermal impacts of rooftop PV on the roof indicates that roofs are cooled when covered by rack-mounted PV with ventilated air gaps and roofs are warmed when covered by flush-mounted PV with no gap. This study investigates the thermal impact of adhesively-mounted rooftop PV, which has a small air gap intermediate between flush-mounted systems (no gap) and rack-mounted systems (> 10 cm gap).

4 Experimental Analysis

Conditioned Test Hut Construction

Two identical wood-framed test huts of 2.44 m x 3.66 m (8 ft. x12 ft.) footprint were located in Fraunhofer CSE's outdoor test facility in Albuquerque, NM. The huts were built according to standard building practice and positioned to minimize solar shading. Each test hut consisted of a 4.5:12 pitched, single-slope, south facing roof with a ceiling separating the attic from the conditioned space below (Figure 1). Design details and thermal insulation levels are presented in Table 1.

15# synthetic felt underlayment was applied over 1.11 cm (7/16 in) thick OSB sheathing. 3-tab composite asphalt shingles (Timberline, GAF, Parsippany, NJ) were installed following standard practice. Asphalt shingles were selected for the roof covering material because it represents an almost 60% of the U.S. roofing market (162.5 million square in 2014) (Freedonia, 2016). Charcoal was chosen as the shingle color as it has a relatively low Solar Reflection Index (SRI) value (ASTM E 1980). Since SRI is a measure of how well a surface reflects solar radiation, shingles with a lower SRI will increase the roof temperature, which may amplify the thermal impact of the adhered module. An increased roof temperature also improves analytic sensitivity.

A [2 rows x 3 columns] array of lightweight PV panels was adhesively-mounted on one of the huts (PV Hut), while the other hut (reference hut) served as a reference (Figure 1b). PV modules are labeled PV1–PV6 (Figure 4). The lightweight (glassless, frameless) PV modules were provided by Lumeta Solar (Sunnyvale, CA; Model LPP-150). The modules consisted of mono-crystalline silicon solar cells encapsulated using standard processes except that a thin polymeric film replaces the front-glass, a semi-rigid back-panel replaces the back-sheet and the aluminum frame is eliminated. The 155W modules are approximately 3 mm (0.12 in.) thick, weigh 5.5 kg (12 lb.) and have dimensions of 1.01 m x 1.01 m. Heliobond® PVA 600BT (Royal Adhesives and Sealants, South Bend, IN), a high performance thermosetting adhesive tape with high tack and adhesion, was used to attach the PV modules to the shingled roof. Adhesive pads of 10 cm x 10 cm size were cut from the adhesive tape and arranged in a [7 rows x 4 columns] array on each PV module. Two different adhesive thicknesses were chosen: the top row of the array was attached with 4.5 mm thick adhesive pads, while the bottom row was attached with 1.5 mm thick adhesive pads. The reference and PV huts are shown in Figure 1c.

A standard roof ventilation strategy was adopted i.e. 1 m^2 of net free-vent area (NFVA) per 300 m^2 of attic space. Equally sized vents were installed on the front and back soffits to allow a total NFVA of approximately 0.03 m^2 in each test hut (Figure 2a). A portable air conditioning (AC) unit (14,000 BTU/h capacity) was installed in each test hut to provide cooling (see Figure 2b). The setpoint was controllable to a temperature resolution of about 0.6°C (1°F).

Measurement Sensors and DAQ Strategy

The temperature and heat flow measurements were performed using thermocouples (TC) and heat flow transducers (HF sensors), respectively. These sensors were placed in various locations of the huts including above and below the shingles and PV modules, in attic space, in conditioned space, inside the attic insulation, on the ceiling surface, and on walls and floor (Figures 4 and 5). Type T thermocouples junctions were welded and prepared in-house using Omega's 24-gauge stranded pair of copper and constantan wires. Surface-mounted TCs were adhered using a fast-cure, thermally conductive epoxy

(Figure 3a). For air temperature measurements, TCs were hung in the locations of interest. To improve the accuracy of the TC measurements, a thermally insulated reference box containing the connection point between the TC wire and lead wires of the voltage measurement device was placed inside the conditioned space. Thermal isolation reduces the influence of the junction potential caused by the dissimilarity of the TC wire and the wire leads.

Thermopile based HF transducers (Concept Engineering, Old Saybrook, CT; Model: F-002-4) with a 5 cm x 5 cm surface area were mounted with a conductive thermal paste to improve thermal contact (Figure 3b). HF sensors were calibrated using a heat flow meter apparatus to correlate the heat flux and Seebeck voltage. The linear correlation was used to convert the HF sensor voltage into the heat flux values.

A data acquisition (DAQ) unit (CR1000, Campbell Scientific, Logan, UT) in combination with a multiplexer (MUX) (AM16/32B, Campbell Scientific) was used to record the temperature and heat flux data. Temperature and heat flux data were scanned in 30-second increments and recorded every minute.

A Kipp and Zonen CMP11 pyranometer and a Vaisala Weather Transmitter WXT520 were mounted near the test hut site to measure and record solar irradiance, wind speed/direction and exterior (ambient) temperature data.

Sensor Arrangement

The sensor arrangement on the roof was given special attention (Figure 4). A vertical array of TCs was installed through the roof cross-section at key locations of both huts: one TC on the module surface, one TC on the shingle surface, one between the overlapping shingle tabs (Figure 3d), and one under the roof deck. A TC array was installed at the center points of PV2 and PV5. TC arrays were also installed at two locations of the roof of the reference hut. In addition, a single TC was attached at the center under modules PV1, PV3, PV4 and PV6 on the shingle surface. One TC each was installed between overlapping shingle tabs located under the adhesive pad adjacent to the centerpoint TC arrays of PV2 and PV5.

Except the roof envelope, the sensor layout in both test huts was kept identical (Figure 5). Three vertically distributed TCs were hung in the center of the interior conditioned space to measure its temperature. Heat flow through the ceiling was measured by two HF sensors placed on the underside of the ceiling. Additional TCs were located on the walls, gable, floor and attic to monitor the temperature of each hut (Figure 5).

Conditioned Space Temperature

During the test hut experiments, the conditioned space temperature was kept at 21.1°C (70°F). It is consistent with the optimum thermal comfort condition as described by the ASHRAE Handbook of Fundamentals (2009).[1] The AC unit setpoint temperatures were adjusted to minimize the differences in the measured conditioned space temperature of the two huts. A comparison of temperatures measured by one of the three TCs located in the conditioned space of the reference and PV huts during a typical week shows a difference of approximately 0.3°C (0.5°F) (Figure 6).

Experiments were conducted for a five-week period from 08/09/2014 to 09/12/2014 representing the late summer in Albuquerque, NM. A summer season testing allowed us to study the thermal impact of

adhesive mounting during a time when temperatures were highest for the year. As described previously, higher temperatures hasten the shingle material degradation; therefore, a summer experiment was designed to investigate the highest-risk scenario from material degradation viewpoint.

5 Results and Discussion

Effect of Adhesive Mounting on Shingle Temperature

Figure 7 compares the temperatures of shingles covered with the adhesive-mounted PV with that of the exposed shingles on the reference hut. The data for covered shingles were collected from the TC arrays located at the center of PV2 and PV5 (Figure 4). The temperature values are from the TCs embedded between overlapping shingle tabs (Figure 3d). This location is insulated from the variable effects of direct exposure to wind and solar radiation and thus provides a cleaner (less-noisy) temperature measurement compared to the signal from TCs placed on the surface of the shingles. The covered shingle data is from a shingle located underneath the air gap (between PV module and shingles) and thus may experience limited convective cooling. Figure 7 shows that the covered shingles are at least 10°C cooler than the exposed shingles on the reference hut during mid-day when the temperature peaks.

Figure 8 quantifies the difference in maximum temperature between the exposed and the covered shingles. In Figure 8, the exposed shingle temperature is represented as the average of thermocouple readings on two locations of the reference hut, while the covered shingle temperature is taken as the average of shingle temperatures under PV2 and PV5 (see Figure 4 for thermocouple locations). Over the one-month period (Aug.-Sept.), the reduction in shingle temperature due to adhesive mounting varied between 4.8°C and 16.1°C, with an average daily peak temperature of 13°C. This reduction in temperature was determined for the hottest part of the Albuquerque summer; it is expected to be less during the cooler months. In comparison, a numerical model, which included PV thermal and electrical performance, determined a reduction of roof temperature due to conventionally mounted PV of 9.4°C in the summer in Tianjin, China (Wilson & Paul, 2011).

The amount of cooling depends on the temperature. In Figure 9, the average temperature of shingles covered by PV2 and PV5 (i.e. covered shingle temperature) is plotted against the average temperature of two exposed shingles on the reference hut (i.e. exposed shingle temperature) for the entire duration of the experiment. The hysteresis in the curve is due to a time-shift (lag) of the covered shingle temperature behind the exposed shingle temperature during the heating stage (as the morning sun heats the system). This lag is reversed during the cooling stage when the exposed shingle temperature drops faster than the covered shingle temperature. The shape of the curve reflects how the irradiation, ambient temperature and wind affect the dynamic heat transfer of the covered and exposed shingles temperatures differently. In general, the temperature of the covered shingles increases with the temperature of the exposed shingles. At lower temperatures of the exposed shingle, the covered shingle appears to closely follow the temperature of the exposed shingles as the hysteresis temperature data appear to lie on 1:1 straight line. However, as the temperature of the exposed shingle increases, there is an increasing and downward separation in the temperature of the covered shingles from the 1:1 straight line, suggesting the cooler temperatures of the covered shingles compared to the exposed shingles. This observation may be attributed to the increasing solar conversion efficiency and air ventilation with increasing temperatures.

Figure 10 depicts a temperature histogram plot of the exposed and covered shingles. There are two distinct peak profiles in the histogram – higher and lower temperature peaks are attributed to daytime and nighttime, respectively. A similar nighttime temperature profile is observed for both exposed and covered shingles. However, for daytime temperatures, the covered shingles are at a significantly lower temperature than the exposed shingle. The maximum temperatures attained in the exposed and covered shingles are at around 73□C and 85□C, respectively. The plot is a clear evidence that the covered shingles remain at a lower temperature than the exposed shingles.

Figure 11 plots the daily peak temperature of the shingles under the PV module vs. the exposed shingles of the reference hut. The daily peak temperature of the covered shingle increases with exposed shingle temperature, but with a slope of <1 (0.79). A linear fit yields the relation:

$$T_{Covered} = 3.5 + 0.79T_{Exposed} \quad (1)$$

where T_{Covered} and T_{Exposed} are the daily peak temperatures of the covered and exposed shingles (in °C), respectively.

The peak cooling effect can be made explicit by rewriting equation (1) in terms of the difference between the temperature of the exposed shingles and the covered shingles:

$$Peak\ Cooling = T_{Exposed} - T_{Covered} = 0.21T_{Exposed} - 3.5 \quad (2)$$

Equation (2) shows that the peak cooling effect is a function of increasing temperature. As the peak daytime temperature of the exposed shingle increases, the peak cooling effect of the adhered module increases. Conversely, as the peak temperature of the exposed shingle decreases, the cooling effect diminishes.

It is important to emphasize that the temperature response of the roof shingle of the test hut is a result of a multitude of environmental conditions such as exterior temperature, solar irradiation, wind speed, interior temperature, level of thermal insulation below the shingle, etc. Therefore, Equations 1 and 2 and related analysis are valid only for the environmental conditions to which the test huts were subjected to during the experiment, such as solar irradiance, ambient temperature, and wind speed and direction as shown in Figures 6–7. These relationships should not be extrapolated beyond the range of peak exposed shingle temperature that were observed as shown in Figure 13.

Effect of Adhesive Mounting on Heat Flow

Figure 12 compares the heat flux through the ceiling into the conditioned space of the PV hut and reference hut. Each heat flux curve represents an average of the two sensors located underneath the ceiling. On a daily basis, the peak of heat flux into the reference hut is found to be much greater than the peak of heat flux into the PV hut conditioned space. The reduction in heat flux through the ceiling caused by adhesive-mounted PV relative to exposed roof may be calculated as the difference in peak ceiling heat flux of the reference and PV huts and then dividing this difference by the peak ceiling heat flux of the reference hut. The percent reduction in the daily peak heat flux through the ceiling calculated in this manner are depicted in Figure 13. A reduction of between 45% and 55% in the ceiling heat flux of the PV hut is noted relative to the reference hut. In fact, the average reduction in peak daily heat flux through the ceiling over the Aug.-Sept. monitoring period is 49%.

Integrating the heat gains i.e. positive heat flows, *Q*", into the conditioned space through the ceiling over time, *t*, yields the roof-generated cooling energy demand:

$$Roof - generated\ Cooling\ Demand = \int_{t=0}^{t_f} Q"(t)dt \qquad (3)$$

where t_f is the monitoring duration. Since the heat flux data is collected in discrete one-minute increments, equation (3) can be rewritten as:

$$Roof - generated\ Cooling\ Demand = \sum_{t=0}^{t_f} Q"(t)\Delta t = 60\sum_{t=0}^{t_f} Q"(t) \qquad (4)$$

The daily roof-generated cooling load for each hut can be calculated using equation (4) and compared. Considering that the ceiling heat flux are lower in the PV hut than the reference hut, it is anticipated that the roof-generated cooling demand will also be lower for the PV hut when compared to the reference hut. Figure 14 plots the percent reduction in daily roof-generated cooling load requirements of the PV hut relative to the reference. A reduction in the cooling load of 49% is evaluated over the Aug.-Sept. monitoring period. The identical reduction in cooling load as in heat flux is attributed to the similar shape of the heat flux curves from the PV hut and reference hut. Due to this similarity, the reduction of the peak heat flux is coincidentally equal to the reduction in hut flux area.

The reduction of cooling load due to rooftop PV will depend on the area of the roof covered by the array. For example, the State of California restricts the PV array coverage to half the total roof area to avoid adding significant inertial mass and seismic lateral loads to the roof (Cain *et al*., 2015). No restriction is placed on any portion of the roof (e.g. a south-facing roof-section) so long as the PV coverage over the *total* roof area does not exceed 50%. 69% of the total area of the single-sloped roof of the PV hut is covered by the PV array, which exceeds the California limit. Since rooftop PV is typically mounted on sun-facing roofs in sunny (warm) climates, their cooling effects are maximized. Thus, maximizing PV array coverage on south-facing roofs not only maximizes energy production but also maximizes the cooling effect.

Effect of Adhesive on Shingle Temperature

During the summer period measurements, the peak daytime temperature of the shingle under the adhesive pad was found to be consistently warmer than that of the shingle under the gap beneath the module (Figure 15). The difference in temperature experienced by a shingle underneath the adhesive compared with a shingle under the gap is up to 6°C during the warmest part of the day (Figure 16). The adhesive pad adds a small thermal resistance which should cause a small decrease in the temperature of the shingle (<1□C) compared to a hypothetical case where the PV module is flush-mounted to the shingle. Lower daytime temperature of the shingle under air gap compared to the shingle under the adhesive pad suggests that the gap, although small, allows for the air flow that removes a portion of the impinging heat from the PV panel above.

The area fraction of the adhesive underneath the adhered modules will significantly affect the heat transfer from the module to the shingles. In this case, approximately 25% of the module back-panel is covered by adhesive pads. Due to the non-flat roof surface, not all of the adhesive makes intimate contact

with the shingle surface, however. The adhesive contact fraction (ACF) depends on the adhesive spacing, pad size, shingle type as well as the applied pressure on installation. The result is that the majority of shingles under module may not be covered with adhesive.

6 Conclusions

A field study to investigate the thermal effects of the adhesive-mounted rooftop PV panels on the underlying roof shingles was performed in Albuquerque, NM. Two identical test hut structures, one with adhesively-mounted lightweight, glass-less PV modules, were exposed to the hot, desert conditions during a five-week summer test period. Asphalt roof shingles under the PV panels were found to be significantly cooler than the exposed shingles. Daily peak temperatures of shingles covered by the PV modules were approximately 13°C lower than exposed shingles during the Aug.-Sept. monitoring period. The cooling effect of the adhered modules increases with increasing temperature. Heat flow to the conditioned space through the ceiling barrier is reduced by 49% compared to the reference hut. The adhesive pads were found to thermally bridge the module with the underlying shingles. Shingles underneath the adhesive pads were up to 6°C warmer than shingles underneath the gap region under the adhered modules.

By acting as a sunshade and intercepting the incident irradiation, the adhered modules *moderate* the energy exchange of the roof with the environment. The seasonal and diurnal temperature swings that exposed shingles experience is dampened. These cooling effects can be maximized by maximizing south-facing roof coverage in warm (sunny) climates. The small gap resulting from the adhesive mounting restricts convective heat flow. A full understanding of the thermal balance would require accounting for the mounting geometry, thermal properties of the system as well as the boundary conditions of substrate, solar isolation and weather conditions.

7 Acknowledgements

The authors would like to thank Lumeta Solar, Royal Adhesives and Sealants, and the U.S. Department of Energy under Award Number DE-EE0006035.

8 DISCLAIMER

Table 1: Basic Design of Test Structures

Envelope Element	Description
Floor	- 2x6 floor joist w/R-19 fiberglass (FG) batt below - Protective layer under floor to hold in R-19 insulation - ¾" T/G plywood - R-10 XPS board on top of floor
Walls	- LP Smartside siding - Wall studs 2x4 @16" o.c. - R-13 FG batt in wall cavity - R-10 XPS board on walls below ceiling joists
Ceiling	- 2x6 @16" o.c. ceiling joists - ½" OSB - R-10 XPS board on ceiling joists below ceiling
Roof	- 2x4 roof rafters @16" o.c. - 7/16" OSB decking - 15# roof membrane - 3-tab FG asphalt shingles; charcoal color

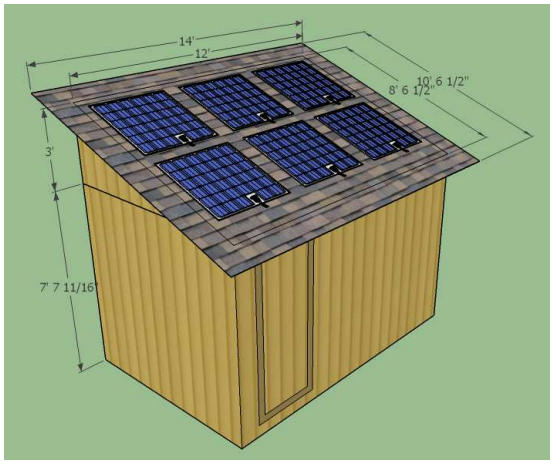

(a)

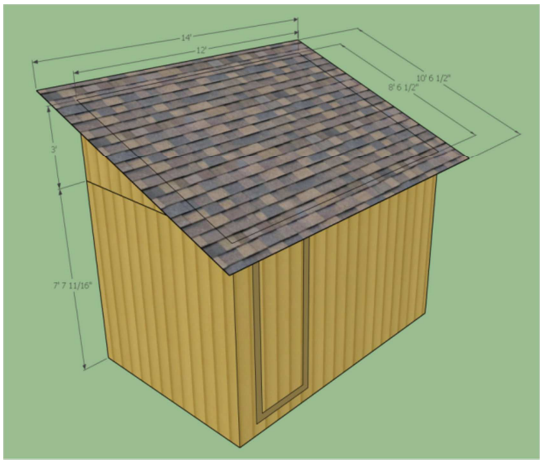

(b)

(c)

(d)

Figure 1: Schematic of (a) PV and (b) reference huts, (c) PV hut (left) and reference hut (right), and (d) adhesive-mounted PV on the roof of the PV hut.

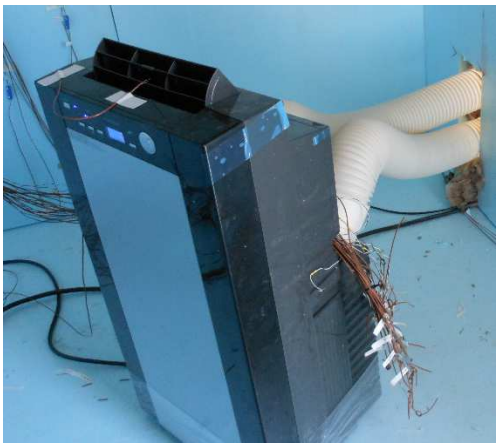

(a) **(b)**

Figure 2: (a) Soffit vent installed in each hut, (b) Portable air conditioning unit.

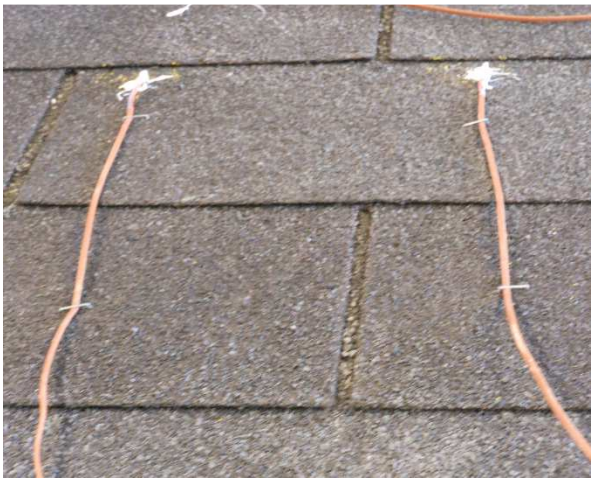

(a)

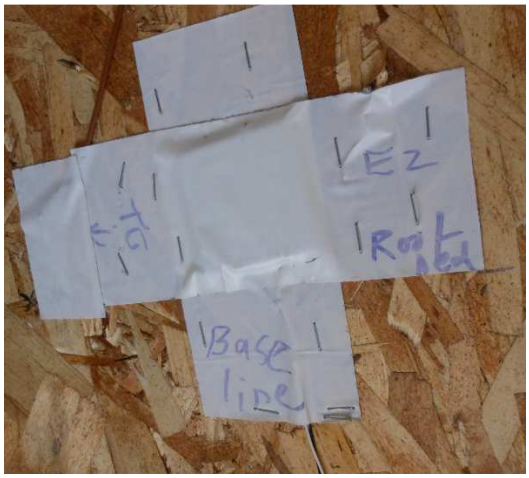

(b)

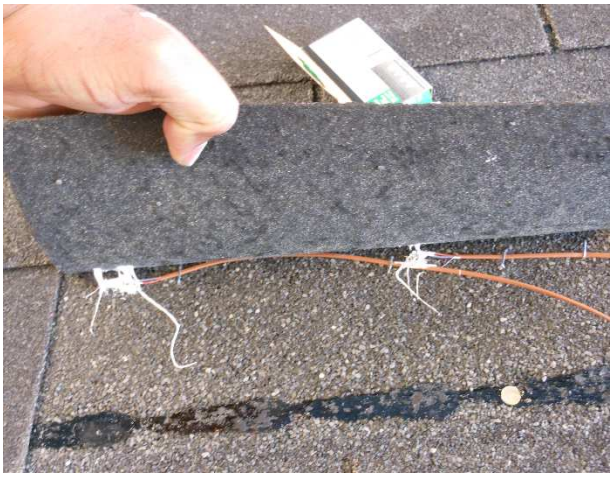

(c)

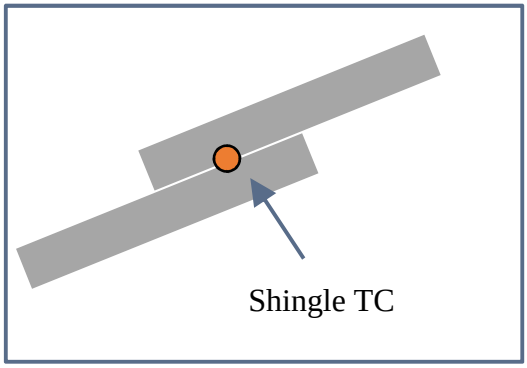

(d)

Figure 3: (a) Thermocouples (TCs) attached to the shingle surface of the PV hut, (b) Heat Flow sensor installed on the underside of the roof deck of the Reference hut, (c) TC attached between overlapping tabs of the shingles and (d) schematic representation of TC embedded between overlapping single tabs.

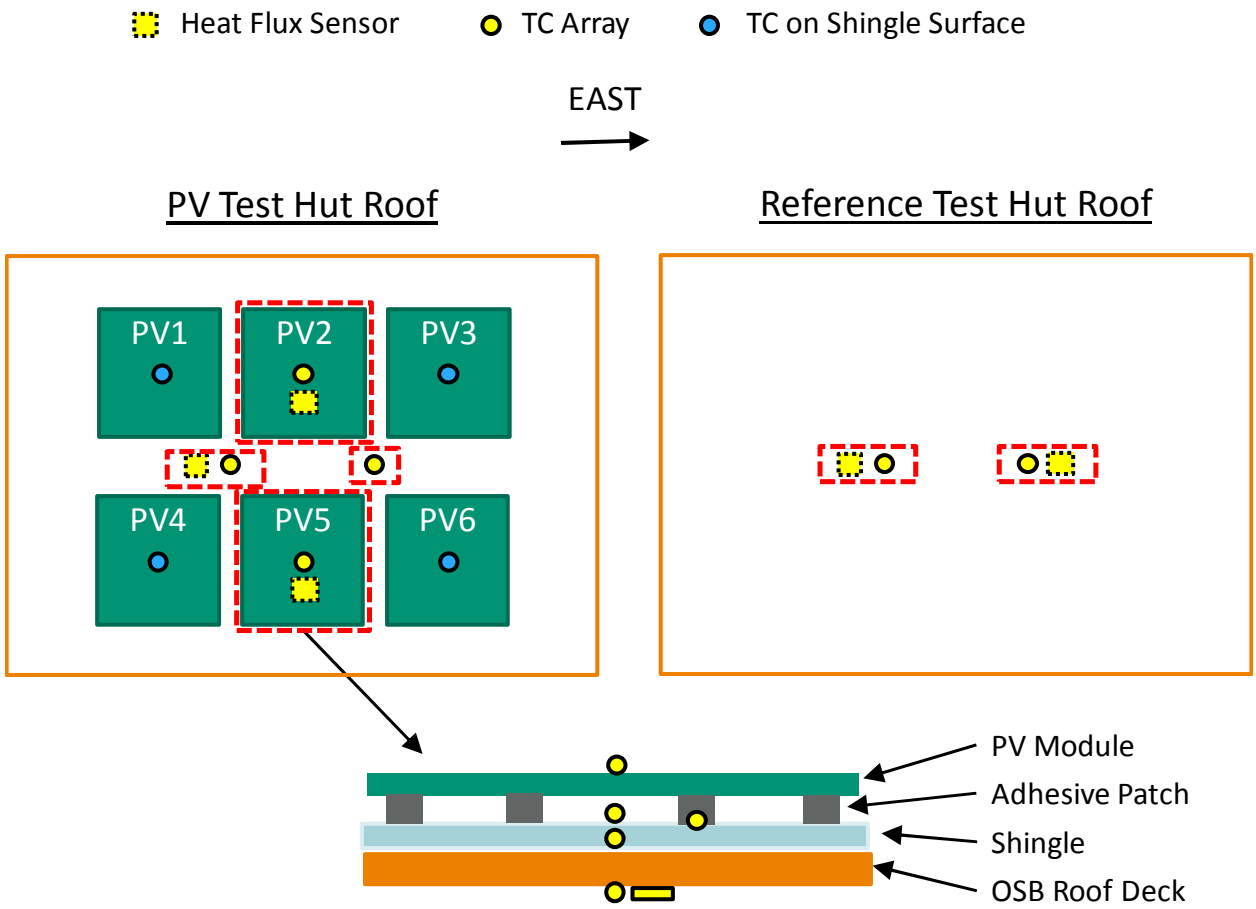

Figure 4: Sensor layout for roof of the Reference and PV test huts. Top row (PV1, PV2, PV3) was attached with 4.5 mm thick adhesive pads; the bottom row (PV4, PV5, PV6) was attached with 1.5 mm adhesive pads. Note that thermocouple (TC) under adhesive pad is mounted for PV2 and PV5 modules only.

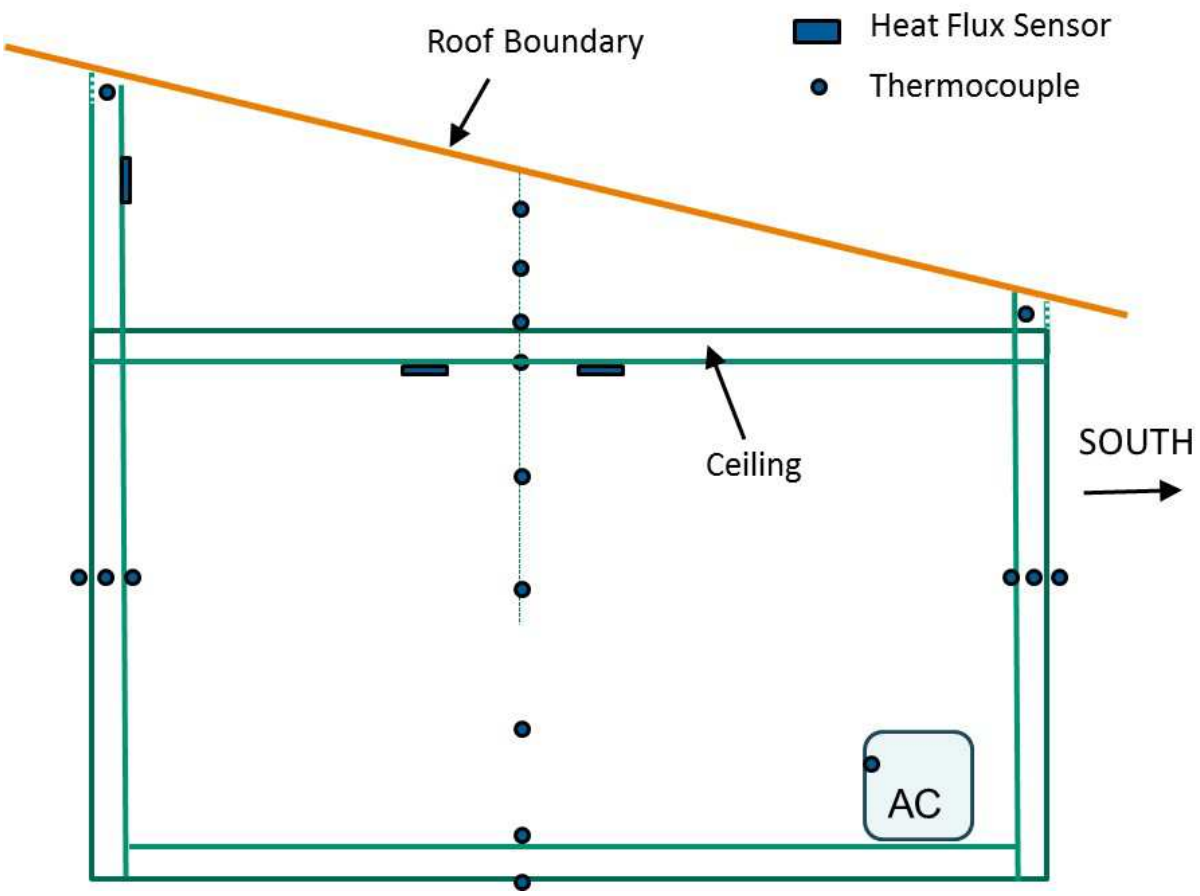

Figure 5: Sensor layout implemented in both the reference and PV test huts below roof boundary. Roof sensor layout for both huts is shown in Figure 4.

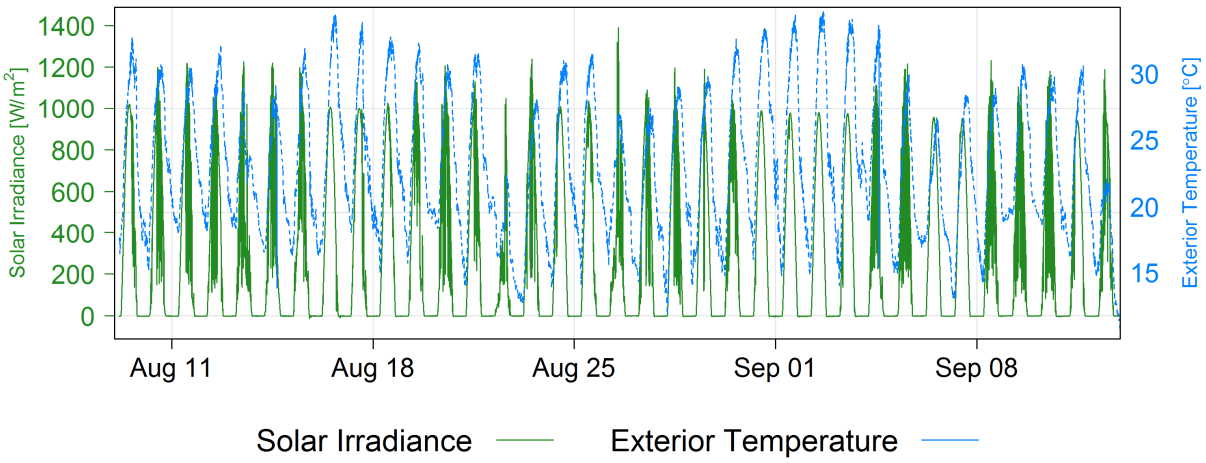

Figure 6: Solar irradiance and ambient (exterior) temperature at the test hut location. A Kipp and Zonen CMP11 pyranometer was used to measure global horizontal irradiance, while a Vaisala Weather Transmitter WXT520 collected exterior temperature data.

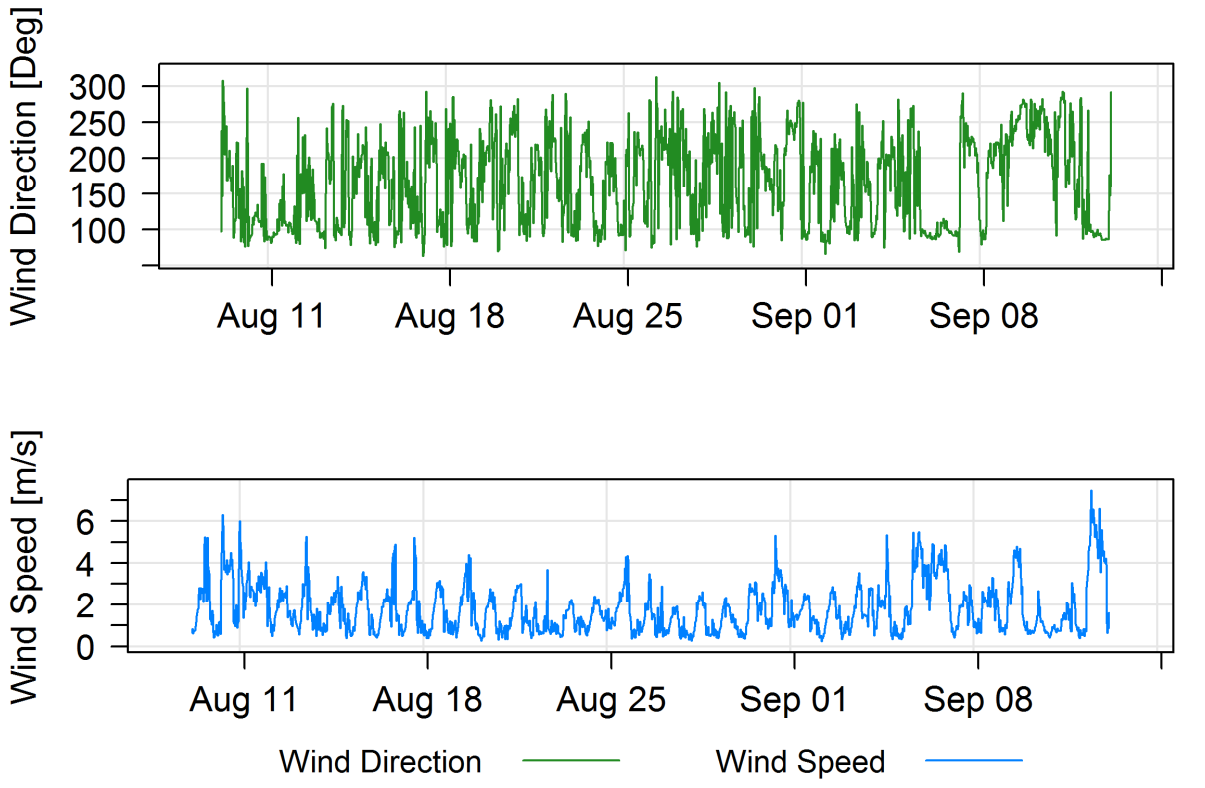

Figure 7: Wind speed and direction at the test hut location as measured by Vaisala Weather Transmitter WXT520.

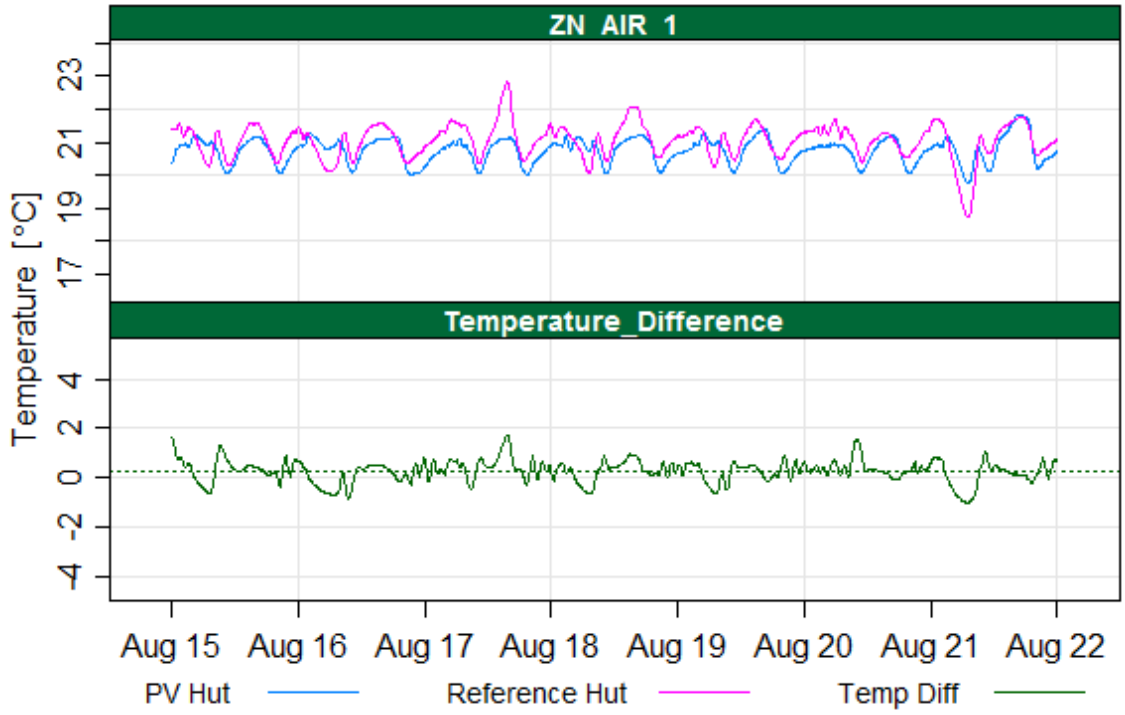

Figure 8: Top: Temperature of the conditioned space in the PV and reference huts as measured by a thermocouple in the center of each hut. Bottom: The difference of the temperatures. The average difference is 0.3°C (0.5°F).

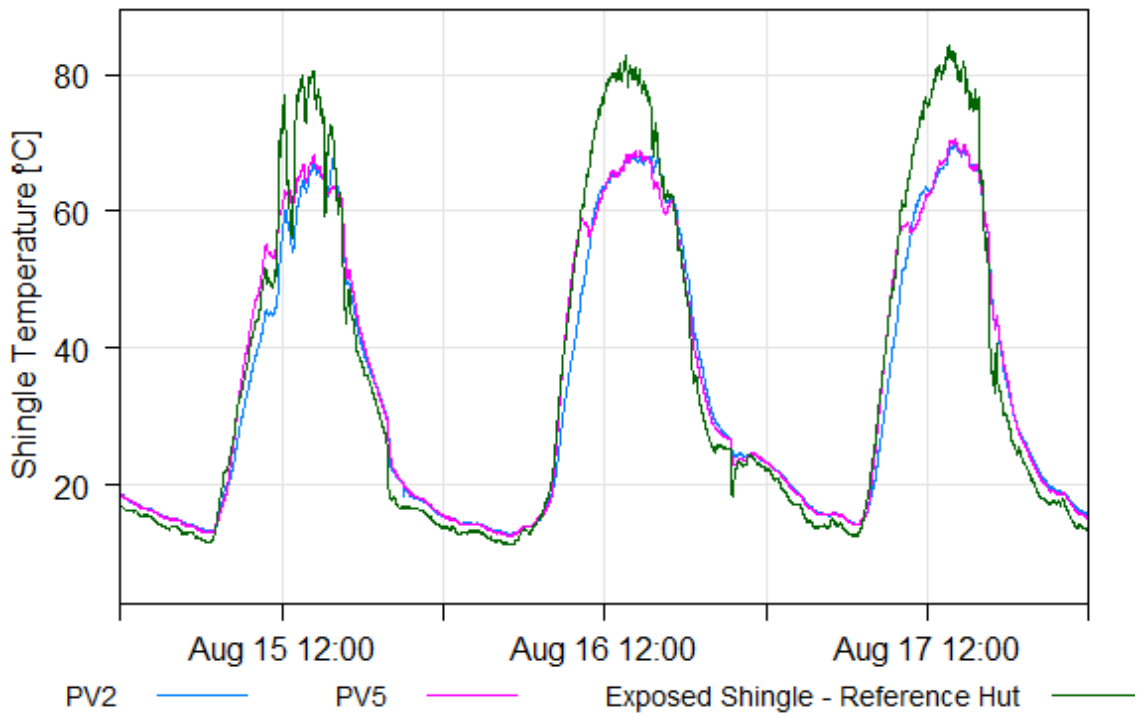

Figure 9: Temperature of shingles under the center of modules PV2 and PV5 as well as the average of two exposed shingles on the reference hut. Note that shingle temperature is represented by a thermocouple embedded between overlapping shingle tabs.

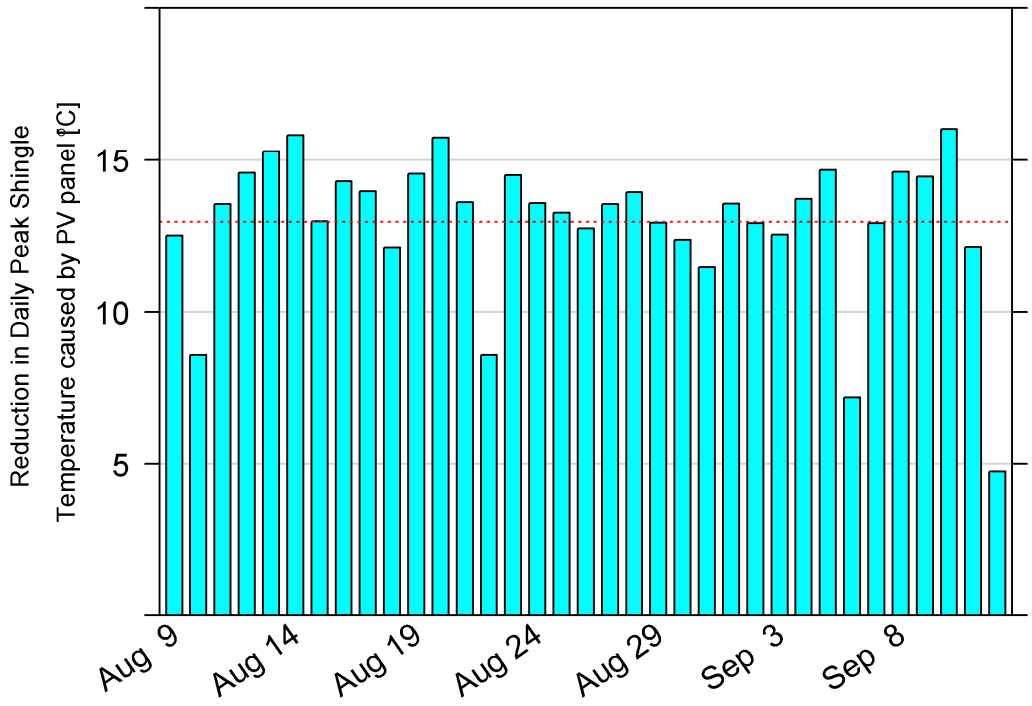

Figure 10: Reduction in daily daytime peak temperature of shingles under PV modules (average of PV 2 and PV5) compared to exposed shingles on the reference hut. The average reduction in peak temperatures is 12.5°C. The horizontal dotted line represents the average reduction.

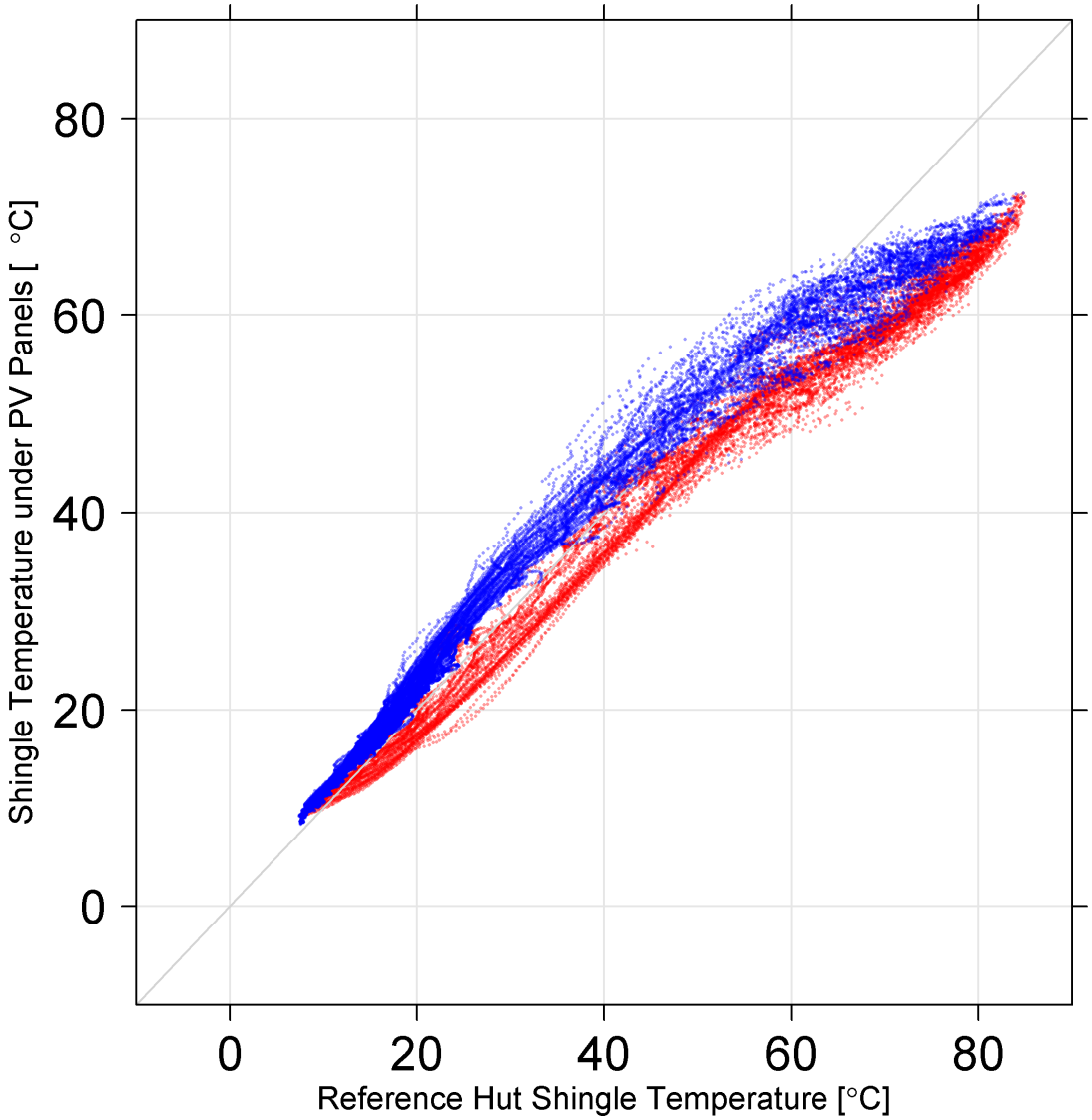

Figure 11: Cross-plot of the average of shingle temperatures under PV2 and PV5 vs. the average of two exposed shingles on the reference hut for the entire duration of the field experiment. In all cases data stem from TCs embedded between shingle tabs (Figure 3d). The data were separated into two time-periods: blue data points representing time between the occurrence of the lowest shingle temperature to the time the highest (peak) shingle temperature was observed in the PV hut for a given day; red data points representing time between the occurrence of the highest shingle temperature to the time the lowest shingle temperature was observed in the PV hut for a given day. The solid line represents a 1:1 straight line.

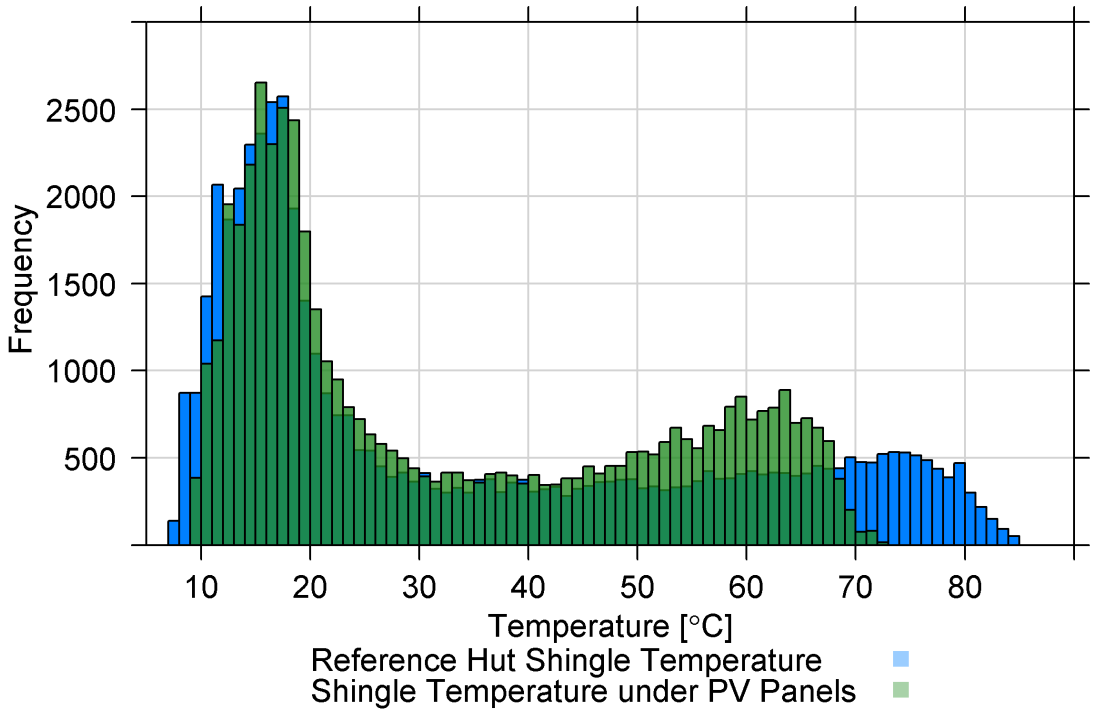

Figure 12: Histogram of temperature of the shingles under the PV modules as well as the exposed shingles on the reference hut. Shingle temperature under PV module is evaluated as the average temperature of shingles located under the center of modules PV2 and PV5; reference hut shingle temperature is evaluated as the average of two exposed shingles on the reference hut.

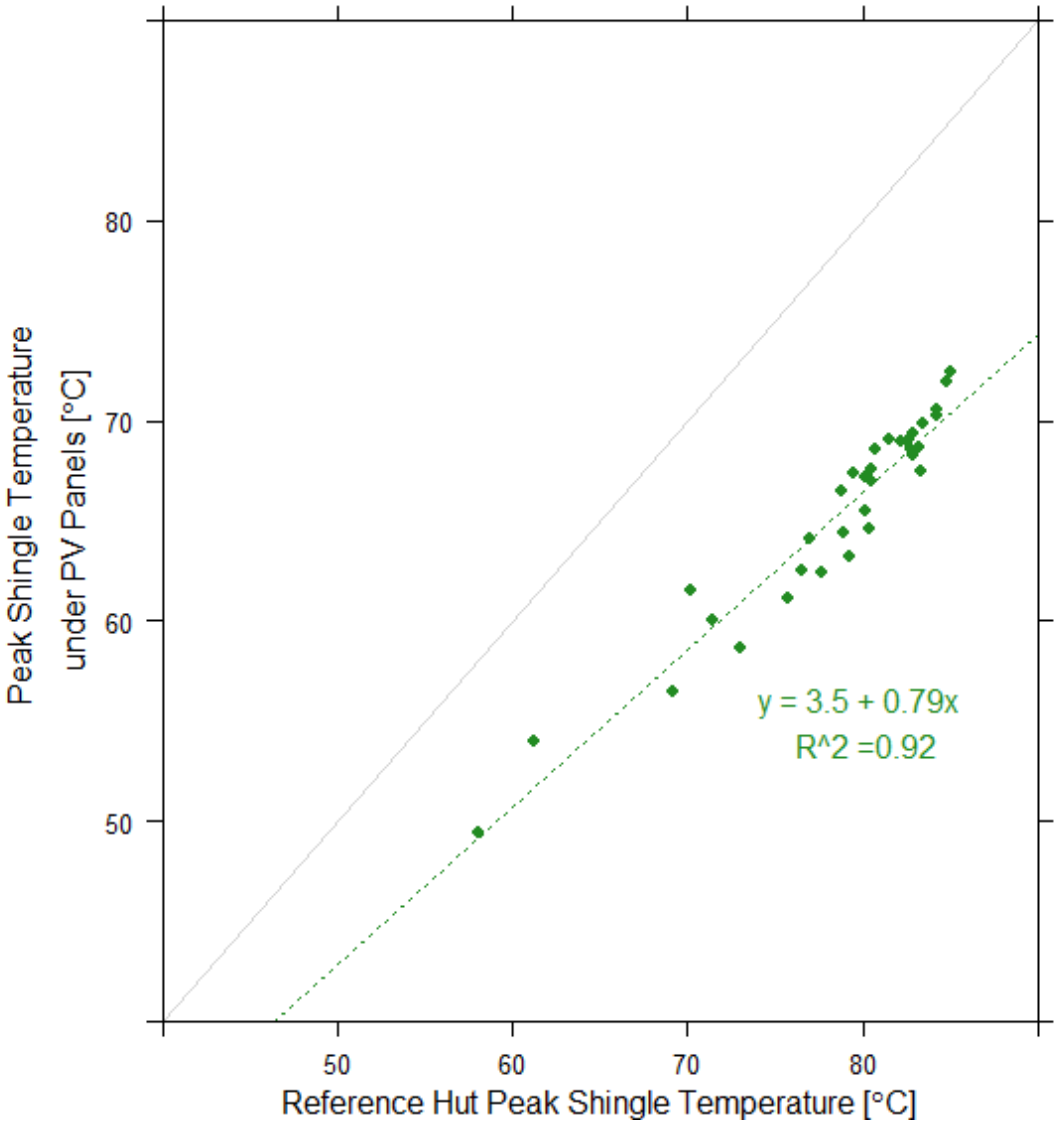

Figure 13: Daily peak temperature of the shingles under the PV modules vs. the exposed shingles on the reference hut. Shingle temperature under PV module is evaluated as the average temperature of shingles located under the center of modules PV2 and PV5; reference hut shingle temperature is evaluated as the average of two exposed shingles on the reference hut. The dotted green line is the linear fit to the data, while solid gray line represents a line with slope of 1.

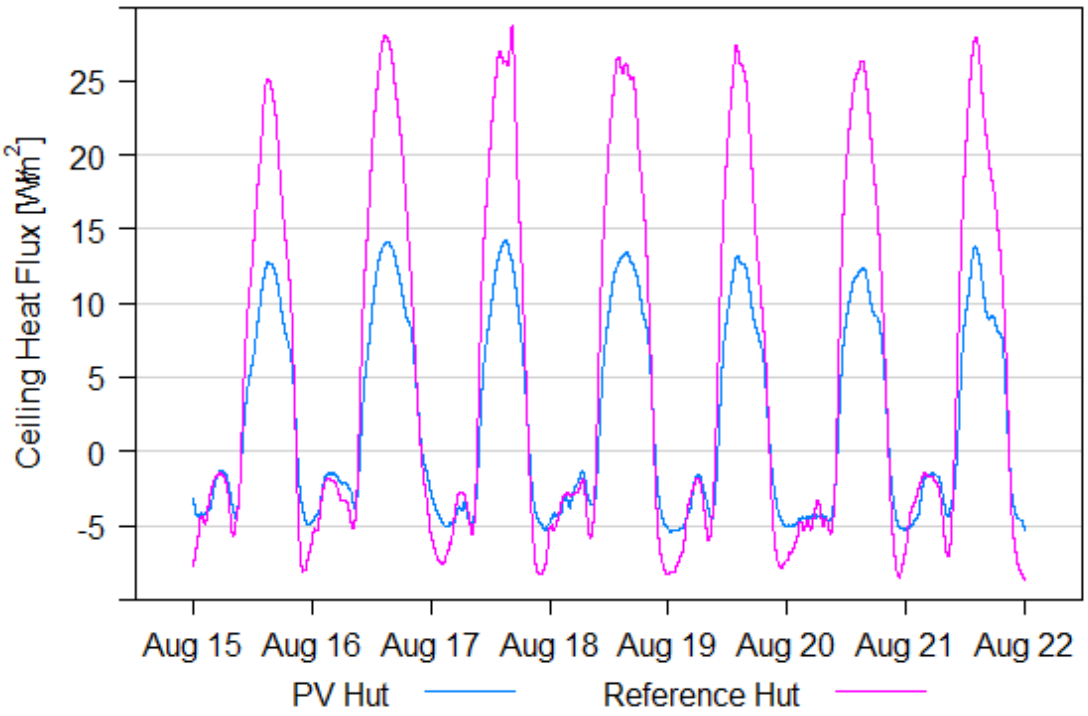

Figure 12: Average heat flux through the ceiling of the reference and PV huts.

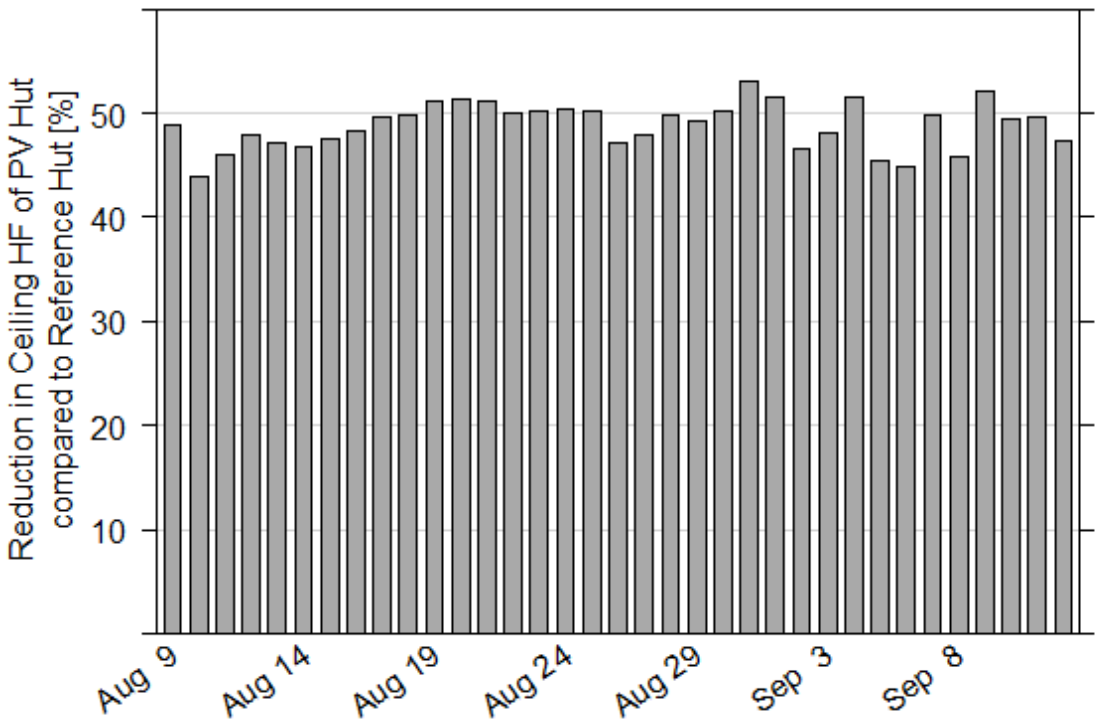

Figure 13: Percent reduction in daytime peak heat flux through the ceiling of the PV hut compared to the reference hut.

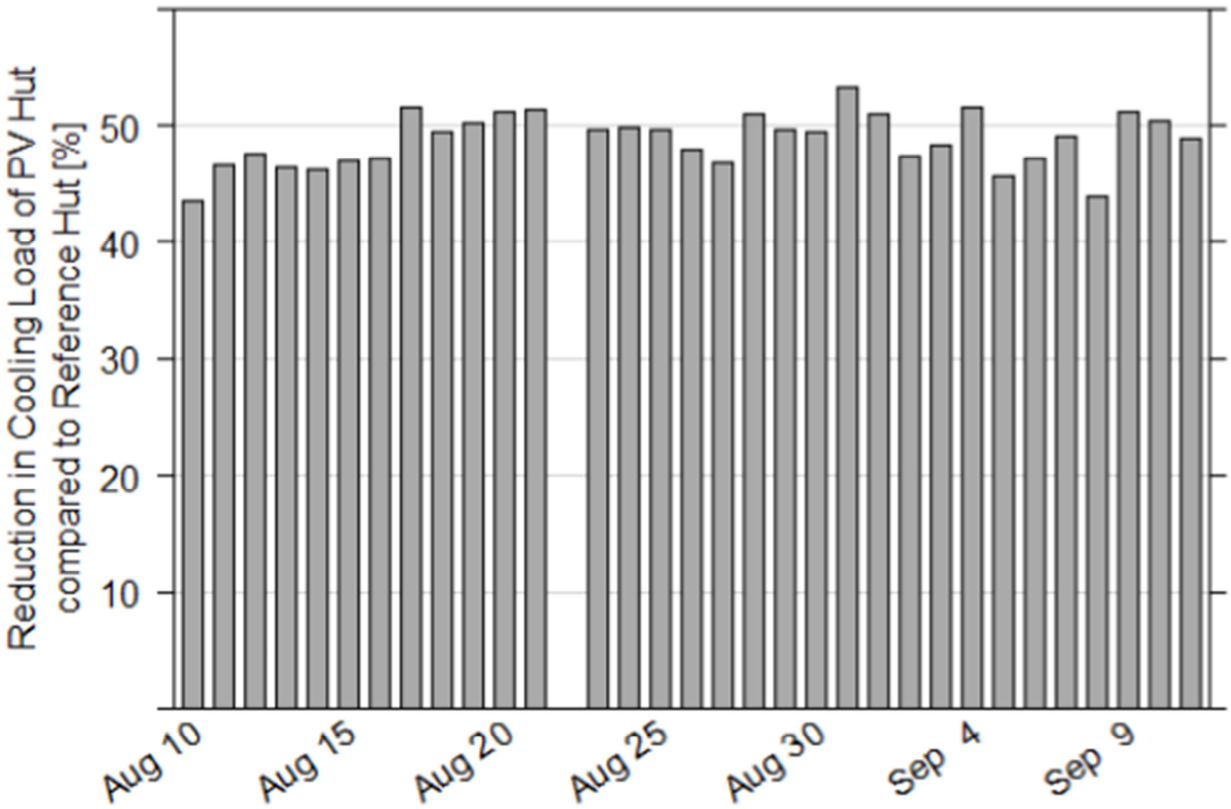

Figure 14: Percent reduction of cooling load through the ceiling envelope of the PV hut compared to the reference hut.

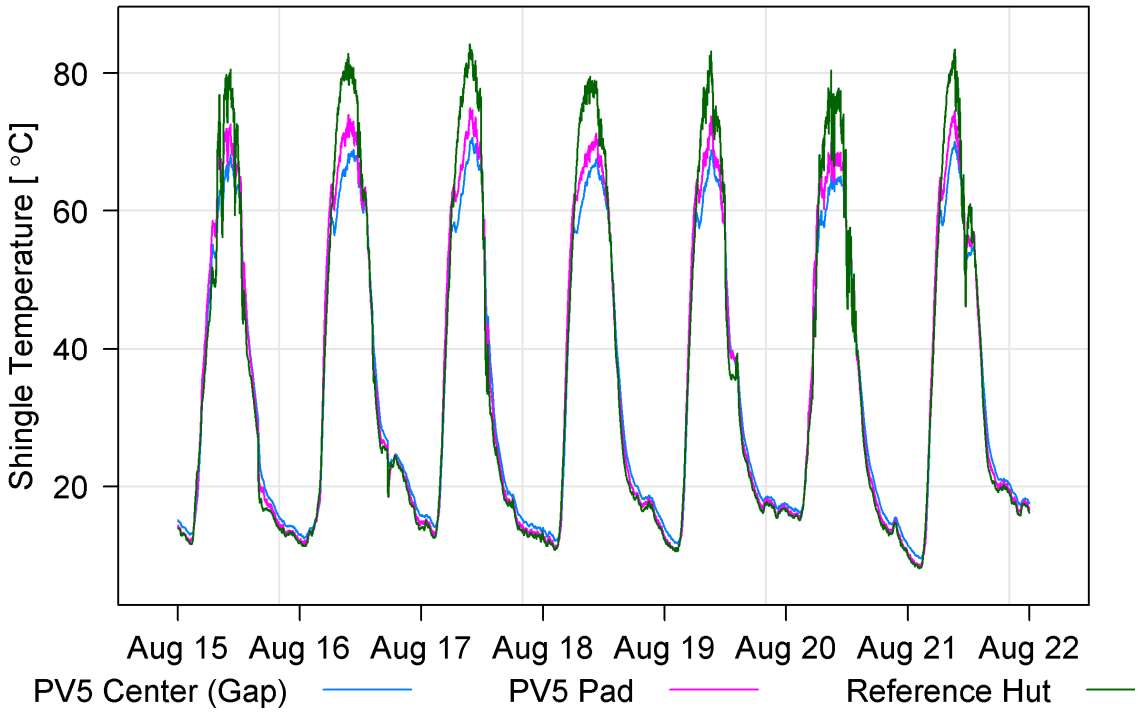

Figure 15: Comparison of shingle temperature of a shingle underneath the air gap with a shingle underneath an adhesive pad for PV5 module in PV hut. Shingle temperature of Reference hut is also included as a comparison. Data stems from TCs embedded between shingle tabs (Figure 3d).

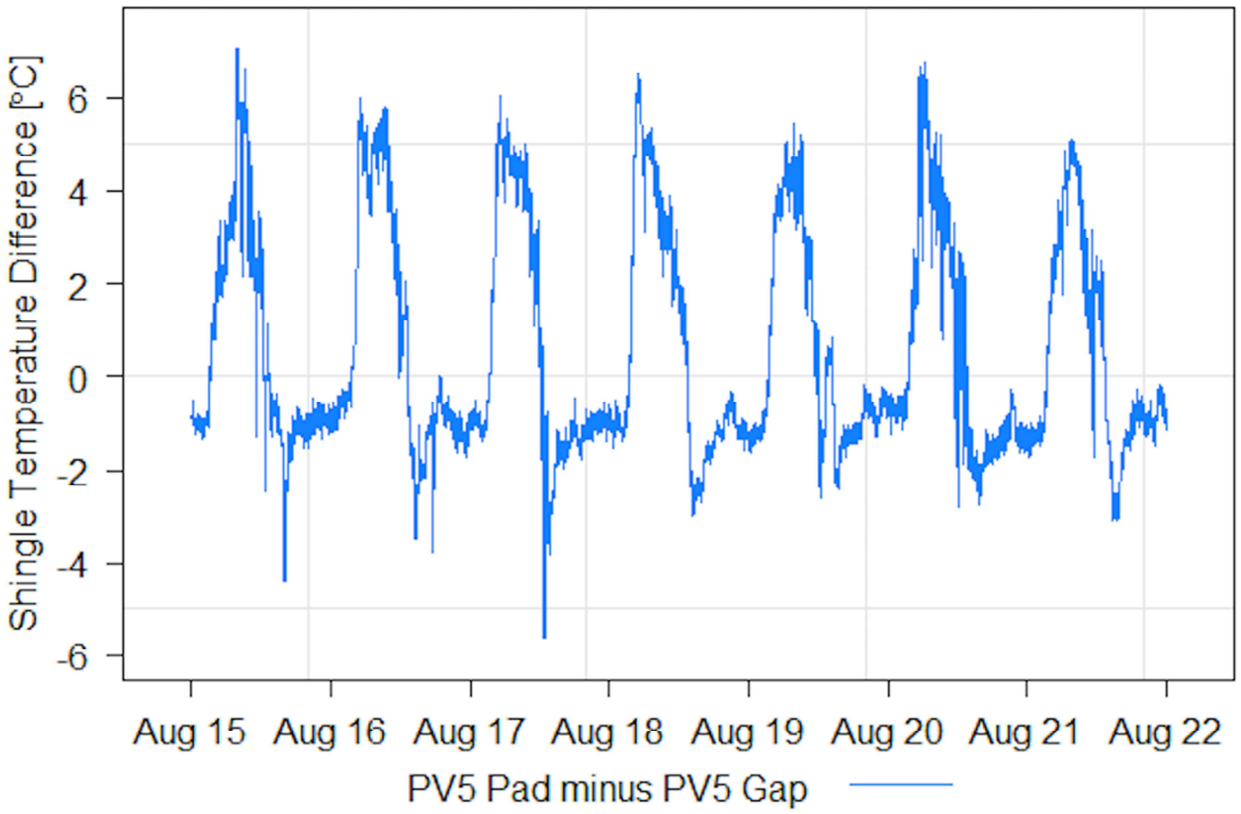

Figure 16: Difference plot showing the increase in temperature of the shingle underneath an adhesive pad compared with a shingle underneath the gap space of PV5 module in PV hut.

REFERENCES

Ardani, K., Seif, D.; Margo, R.; Morris, J.; Davidson, C.; Truitt, S.; Torbert, R.; 2013. Non-Hardware ("Soft") Cost-Reduction Roadmap for Residential and Small Commercial Solar Photovoltaics, 2013–2020. (Rep. No. NREL/TP-7A40-59155).

ARMA Technical Bulletin; 1996. Application of asphalt shingles over insulation or insulated decks. ARMA Form No. 209-RR-86.

ASHRAE; 2009. *Handbook of Fundamentals*. Chapter 9 – Thermal Comfort.

ASTM E 1980; 2011. Standard Practice for Calculating Solar Reflectance Index of Horizontal and Low-Sloped Opaque Surfaces. http://www.astm.org/Standards/E1980.htm.

Barbose, G.; Darghouth, N.; Weaver, S.; Wiser, R.; 2013. Tracking the Sun VI: An Historical Summary of the Installed Price of Photovoltaics in the United States from 1998 to 2012, Report. https://emp.lbl.gov/sites/all/files/lbnl-6350e.pdf

Barbose, G. & Darghouth, N.; 2015. Tracking the Sun VIII: The Installed Price of Residential and Non-Residential Photovoltaic Systems in the United States. *Lawrence Berkeley National Laboratory (LBNL)*. https://emp.lbl.gov/publications/tracking-sun-viii-installed-price

Berdahl, P.; Akbari H.; Levinson R.; Miller, W. A.; 2008, April. Weathering of roofing materials—an overview. *Construction and Building Materials*, **22(4)**, 423–433.

Beutner, V.; Singh, R.; Stark, C; (submitted, 2017). Temperature and Power Study of Adhered and Racked Double Glass Photovoltaic Modules. *44th IEEE Photovoltaic Specialist Conference*, submitted, 2017.

Bigot D.; Miranville F.; Boyer H.; Fakra A.H.; 2009. A nodal thermal model for photovoltaic systems: impact on building temperature fields and elements of validation for tropical and humid climatic conditions. *Energy and Buildings*, **41, Issue 1**, 1117-1126.

Brinkworth, BJ.; Sandberg, M.; 2006. Design procedure for cooling ducts to minimize efficiency loss due to temperature rise in PV arrays. *Solar Energy*,80:89-103.

Buildings Energy Databook; 2010. U.S. Department of Energy – Energy Efficiency and Renewable Energy. http://buildingsdatabook.eren.doe.gov/TableView.aspx?table=2.1.15

Cain, J.; Hanson, R.; Lai, J.; Maffei, J.; Rogelstad, J.; Scheel, N.; Wagner, A.; Wolfe, J.; 2015. Structural Technical Appendix for Residential Rooftop Solar Installations. *California Governor's Office of Planning and Research 2015*.

Cash, C. G.; 2000. Estimating the durability of roofing systems in *Durability 2000: Accelerated and Outdoor Weathering Testing*, STP 1385, Ketola, W. D.; Evans, eds. J. D.; American Society for Testing and Materials, Philadelphia, 165–169.

Dominguez, A.; Kleissl, J.; Luvall, J.C.; 2011. Effects of solar photovoltaic panels on roof heat transfer. *Solar Energy*, **85(9)**, 2244–55.

Dubey, S.; Sarvaiya, J. N.; Seshadri, B.; 2013. Temperature dependent photovoltaic (PV) efficiency and its effect on PV production in the world - A review. *Energy Procedia*, vol. **33**, pp. 311–321.

Fraunhofer CSE; 2017. Plug and Play PV System. http://www.cse.fraunhofer.org/pnp

Freedonia; 2016. Roofing - Demand and Sales Forecasts, Market Share, Market Size, Market Leaders. http://www.freedoniagroup.com/Roofing.html

Gagnon, P.; Margolis, R.; Melius, J.; Phillips, C.; Elmore, R.; 2016, March. Rooftop Solar Photovoltaic Technical Potential in the United States: A Detailed Assessment. (Rep. No. NREL/TP-6A20-65298).

Gan, G.; 2009. Effect of air gap on the performance of building-integrated photovoltaics. *Solar Energy*, **34(7)**, 913–21.

Gan, G.; 2009. Numerical determination of adequate air gaps for building-integrated photovoltaics. *Solar Energy*, **83(8)**,1253–73.

Harris, G.; 2016. Will railed solar racking systems soon be obsolete in the residential sector? *Greentech Media*. http://www.greentechmedia.com/articles/read/the-death-of-rails.

Hirunlabh, J.; Wachirapuwadon, S., Pratinthong, N., Khedari, J., 2001. New configurations of a roof solar collector maximizing natural ventilation in *Building and Environment.* ***36*****, no. 3**, 383-391.

Honeker, C.; Fuller, E.; Watts, A.; Booth, D.; Flaherty, B.; Mao, E.; 2016. Reducing Installed Costs of Residential Solar by the Use of Adhesive Mounted Lightweight Solar Modules in *43rd IEEE Photovoltaic Specialist Conference*.

Kann, S.; Shiao, M.; Honeyman, C.; Litvak, N.; Jones, J.; Cooper, L.; Kimbis,T.; Baca, J.; Rumery, S.; Holm A.; 2015. US Solar Market Insight Year in Review 2015, *SEIA/GTM Research*. http://www.seia.org/research-resources/solar-market-insight-2015-q4.

Kośny, J.; Biswas, K.; Miller, W.; Kriner, S.; 2012. Field thermal performance of naturally ventilated solar roof with PCM heat sink. *Solar Energy*, **86**, 2504–14.

Mei, L.; Infield, D. G.; Gosttschalg, R.; Loveday, D. L.; Davies, D.; Berry, M.; 2009. Equilibrium thermal characteristics of building integrated photovoltaic tiled roof. *Solar Energy*, vol. **83**, pp. 1893-1901.

Morris, J.; Calhoun, K.; Goodman, J.; Seif, D.; 2013. Reducing Solar PV Soft Costs - A Focus on Installation Labor. Rocky Mountain Institute (RMI). http://www.rmi.org/Knowledge-Center/Library/2013-16_SimpleBoSRpt.

Morris, J.; Calhoun, K.; Goodman, J.; & Seif, D.; 2014. Reducing Solar PV Soft Costs : A Focus on Installation Labor. *IEEE 40th Photovoltaic Specialist Conference Proceedings*, pp. 3356–3361.

Moshfegh, B.; Sandberg, M.; 1998. Flow and heat transfer in the air gap behind photovoltaic panels. *Renewable and Sustainable Energy Reviews* **2 (3)**, 287–301.

Samady, M. F.; 2011. Photovoltaic Roof Heat Flux. M.S. Thesis submitted to Engineering Science Department, UC San Diego.

Sandberg, M.; Moshfegh, B.; 1998. Ventilated-solar roof air flow and heat transfer investigation. *Renewable Energy*, **15 (1–4)**, 287–292.

Shukla, N.; Watts, A.; Honker, C.; Kośny, J.; In publication. Hygrothermal Impact of Adhesive-applied Rooftop PV. ASTM C16 Special Technical Paper (STP) 1599 on *Symposium on Advances in Hygrothermal Performance of Building Envelopes: Materials, Systems and Simulations*.

Terrenzio, L.; Harrison, J.; Nester, D.; Shiao, M.; 1998. Natural vs. Artificial Aging: Use of Diffusion Theory to Model Asphalt and Fiberglass-Reinforced Shingle Performance. *Proceedings of the Fourth International Symposium on Roofing Technology*, vol. **31 (7)**, pp. 66-74.

Tian W.; Wang Y.; Xie Y.; Wu D.; Zhu L.; Ren J.; 2007. Effect of building integrated photovoltaics on microclimate of urban canopy layer. *Building and Environment* **42 (5)**, 1891-1901.

Trinuruk, P.; Sorapipatana, C.; Chenvidhya, D.; 2007. Effects of Air Gap Spacing between a Photovoltaic Panel and Building Envelope on Electricity Generation and Heat Gains through a Building. *Asian Journal of Energy Environ*, vol. **8,** Issue 1 and 2, pp. 73-95.

Uni-Solar; 2005. Field Applied PV Laminate Installation Guide for Steel Roof Systems. [online]. http://www.solarcellsales.com/techinfo/docs/PVLdatasheet.pdf

Wilson, M. J.; Paul, M. C.; 2011. Effect of mounting geometry on convection occurring under a photovoltaic panel and the corresponding efficiency using CFD. *Solar Energy*, vol. **85**, pp. 2540-50.

Yang, HX.; Burnett J.; Zhu, Z.; *et al.;* 2001. A simulation study on the energy performance of photovoltaic roofs. *ASHRAE Transactions*, **107**, part 2:129-135.